Rheology of colloidal gas aphrons (microfoams) made from different surfactants

Jiafei Zhao [a], Saurabh Pillai [b], Laurent Pilon [b],*

[a] *Zhejiang University, State Key Laboratory of Clean Energy Utilization, Hangzhou, 310027, PR China*
[b] *University of California, Los Angeles, Mechanical and Aerospace Engineering Department, 420 Westwood Plaza, Los Angeles, CA 90095-1597, United States*

ARTICLE INFO

ABSTRACT

This paper extends our previous study on microfoam rheology made from non-ionic (Tween 20) surfactants to ionic surfactants. Anionic (sodium dodecyl sulfate) and cationic (cetyl trimethylammonium bromide) surfactants were used to generate microfoams by stirring an aqueous surfactant solution at high speed in a baffled beaker. Pipe flow experiments were performed in cylindrical stainless steel pipe 1.5 mm in diameter under adiabatic and fully developed laminar flow conditions. The porosity ϕ, bubble size distribution, Sauter mean radius r_{32}, surface tension σ, and pH was reported for each solution. The porosity varied between 0.54 and 0.72 while the Sauter mean radius ranged from 28 to 48 μm. Zero slip velocity was assumed to prevail at the foam–wall interface as previously observed and reported in the literature for stainless steel pipes. Volume equalized method was used to analyze the data obtained from pipe flow viscometer. In all cases, microfoams behave as a shear thinning fluid. The results suggest that the dimensionless wall shear stress $\tau_w^* = \tau_w r_{32}/\sigma\varepsilon$ is proportional to $(Ca^*)^m$ defined as $Ca^* = \mu_\ell r_{32}\dot{\gamma}_a/\sigma\varepsilon$ where τ_w is the wall shear stress, $\dot{\gamma}_a$ is the shear rate, σ is the surface tension, μ_ℓ is the liquid velocity, and $\varepsilon = 1/(1-\phi)$ is the specific expansion ratio. The average value of the power–law index m was found to be 0.64 ± 0.04 with 95% confidence interval.

1. Introduction

This study extends our previous investigation [1] into the rheology of colloidal gas aphrons (CGA), also called microfoams. In Ref. [1], microfoams were formed with aqueous non-ionic surfactant solutions of Tween 20 at different concentrations. The microfoams consisted of closely packed spherical bubbles 10–100 μm in diameter while porosity ranged from 0.63 to 0.73. First, it was established that (i) no slip velocity is present at the stainless steel pipe wall, (ii) CGA can be considered as a shear thinning fluid, (iii) pipe shape and diameter have no effect on the CGA rheology, and (iv) compressibility effects can be accounted for through the volume equalization approach [2].

The present study aims to assess whether similar qualitative and quantitative results prevail for microfoams made with different surfactants and having porosity between 0.54 and 0.72. Our choice focused on anionic surfactant sodium dodecyl sulfate (SDS) and cationic surfactant cetyl trimethylammonium bromide (CTAB) because both are commonly used in CGA applications [3–7].

2. Background

2.1. Foam rheology

Liquid foams are known to be non-Newtonian fluids. Rheological models have been reviewed in detail previously [1] and need not be repeated. Only the models relevant to the present study will be discussed briefly. First, the pseudo-plastic power–law model is expressed as:

$$\tau_w = K_P \dot{\gamma}_w^n = K_P' \dot{\gamma}_a^n = \mu_e \dot{\gamma}_a \tag{1}$$

where τ_w is the wall shear stress, $\dot{\gamma}_w$ is the true wall shear rate, and $\dot{\gamma}_a$ is the apparent shear rate. The empirical constants K_P and n are the so-called flow consistency and flow behavior, respectively. The true wall shear rate $\dot{\gamma}_w$ can be derived from $\dot{\gamma}_a$ through the Rabinowitsch–Mooney relationship [8],

$$\dot{\gamma}_w = \left(\frac{3n+1}{4}\right)\dot{\gamma}_a \quad \text{and} \quad K_P' = K_P\left[\frac{3n+1}{4n}\right]^n \tag{2}$$

Alternatively, the Herschel–Bulkley model accounts for the possible existence of yield stress τ_0 and is expressed as

$$\tau_w = \tau_0 + K_{HB}\dot{\gamma}_w^{n'} \tag{3}$$

where K_{HB} is the consistency, and n' is the power–law index. It has been used successfully for macrofoams made of aqueous polymer solutions [9,10].

* Corresponding author. Tel.: +1 310 206 5598; fax: +1 310 206 2302.
E-mail address: pilon@seas.ucla.edu (L. Pilon).

Nomenclature

$B(x)$	empirical function in $\tau_w^* = B(x)(\text{Ca}^*)^m$
$C(x)$	empirical function in $\tau_w^* = C(x)(\text{Ca}^*)^{2/3}$
Ca^*	volume equalized Capillary number, $\text{Ca}^* = \mu_\ell r_{32}\dot{\gamma}_a/\varepsilon\sigma$
Ca	Capillary number, $\text{Ca} = \mu_\ell r_{32}\dot{\gamma}_a/\sigma$
Ca^+	Capillary number based on bubble velocity, $\text{Ca}^+ = \mu_\ell u_b/\sigma$
Ca'	Capillary number based on slip velocity, $\text{Ca}' = \mu_\ell u_s/\sigma$
D_h	hydraulic diameter (m)
K_{HB}, K_P, K_{VE}	flow consistency for various models
L	distance between pressure sensors (m)
m	power–law index in $\tau_w^* = B(x)(\text{Ca}^*)^m$
$\dot{m}$	mass flow rate (kg/s)
n, n', n''	flow behavior indices
ΔP	pressure drop (Pa)
$\dot{Q}$	volumetric flow rate (m^3/s)
r_{32}	Sauter mean bubble radius (m)
t	time (s)
u_s	wall slip velocity (m/s)
u_b	average bubble velocity (m/s)
x	surfactant mass fraction (wt.%)

Greek letters

ε	specific expansion ratio, $\rho_\ell/\rho_{CGA} = 1/(1-\phi)$
ϕ	volume fraction of air in CGA or porosity, V_g/V_{CGA}
$\dot{\gamma}_a$	apparent shear rate (1/s)
$\dot{\gamma}_w$	true wall shear rate (1/s)
μ	dynamic viscosity (Pa s)
ρ	density (kg/m^3)
σ	surface tension (N/m)
τ_w	wall shear stress (Pa)
τ_w^*	dimensionless volume equalized wall shear stress $(\tau_w^* = (\tau_w r_{32})/\sigma\varepsilon)$
τ_0	yield shear stress (Pa)

Subscripts

CGA	refers to CGA
f	refers to working fluid in general (water or CGA)
g	refers to gas in microfoams
ℓ	refers to the liquid phase or single phase water
w	refers to the wall

Similarly, the volume equalization method has been used to analyze foams and microfoams rheology [1,2,11,12]. It accounts for compressibility effects through the use of the specific expansion ratio ε defined as the ratio of the densities of the liquid phase and microfoams, i.e., $\varepsilon = \rho_\ell/\rho_{CGA} = 1/(1-\phi)$ where ϕ is the gas volume fraction or porosity. Then, the volume equalized shear stress is given by [2],

$$\frac{\tau_w}{\varepsilon} = K_{VE}\left(\frac{\dot{\gamma}_w}{\varepsilon}\right)^{n''} \tag{4}$$

where K_{VE} and n'' are constants determined empirically.

Alternatively, Schwartz and Princen [13] expanded Bretherton's model [14], predicting the pressure drop along a single bubble in capillary tubes, to 2D-foams with monodispersed hexagonal cells and large porosity subjected to small oscillatory deformations caused by a periodic uniaxial strain lower than the elastic limit. The resulting model predicts that the wall shear stress is expressed

as [15],

$$\tau_w = \tau_0 + C(\phi)\frac{\sigma}{r_{32}}\text{Ca}^{2/3} \tag{5}$$

where r_{32} is the Sauter mean bubble radius, and σ is the surface tension of the gas/liquid interface. The Capillary number Ca is defined as,

$$\text{Ca} = \frac{\mu_\ell r_{32}\dot{\gamma}_a}{\sigma} \tag{6}$$

where μ_ℓ is the viscosity of the liquid phase. However, as noted by Denkov et al. [16], Eq. (5) is not valid for continuous shear flow. On the other hand, Cantat and co-workers [17,18] showed that the pressure drop along a chain of a few large polyhedral bubbles flowing in a narrow rectangular channel was proportional to $(\text{Ca}^+)^{2/3}$ for $\text{Ca}^+ \ll 1$ and defined as $\text{Ca}^+ = \mu_\ell u_b/\sigma$ where u_b is the average bubble velocity [17]. Simultaneously, Denkov et al. [16,19] developed a model accounting for the viscous friction over the entire area separating the bubbles from the wall and distinguishing between tangentially mobile and immobile bubble surface. Surface mobility depends on various parameters but most importantly on the surface dilatational modulus E_S whose large value ensures tangentially immobile surface. Their models predict the foam-wall shear stress in 3D-foams with immobile and mobile bubble surfaces, respectively as [16],

$$\tau_w = C_{IM}\left(\frac{\sigma}{r_{32}}\right)\frac{(0.511 - 0.731\phi)}{(1 - 5.12\phi + 4.03\phi^2)}(\text{Ca}')^{1/2}$$
$$\text{for } 0.73 < \phi < 0.99 \text{ and } E_S \geq 60\,\text{mN/m} \tag{7}$$

$$\tau_w = 3.0C_M\left(\frac{\sigma}{r_{32}}\right)\sqrt{1 - 3.2\left(\frac{\phi}{1-\phi} + 7.7\right)^{-1/2}}(\text{Ca}')^{2/3}$$
$$\text{for } 0.71 < \phi < 1 \text{ and } E_S < 60\,\text{mN/m} \tag{8}$$

where C_{IM} and C_M are empirical constants and Ca' is the capillary number defined as $\text{Ca}' = \mu_\ell u_s/\sigma$ where u_s is the relative velocity between the foam and the wall [16]. The models and more specifically, the power–law index associated with Ca' and equal to either 1/2 or 2/3, was validated against experimental data obtained with a shear rheometer and aqueous foams made from various surfactant solutions with porosity of 0.90 ± 0.01 and Sauter mean radius between 35 and 200 μm [16,20]. The authors determined experimentally that $C_{IM} \approx 4.6$ and $C_M \approx 3.9$ [16]. Note that the range of porosity for which these models are valid corresponds to relatively dry foams ($\phi > 0.7$) with non-spherical bubbles.

Experimentally, care should be taken to isolate the rheological properties of CGA or foams from transient phenomena such as liquid drainage and bubble coalescence. In particular, the foam porosity and bubble size distribution should remain the same during the course of the measurements. Flow pipe viscometers appear to offer the best compromise between these considerations and accuracy requirements and have been used by various authors for studying rheology of macrofoams [2,11,12] and CGA [1,21].

The present study differs from previous studies and in particular Ca' those of Denkov and co-workers' [16,19,20] in that it investigates 3D microfoams having relatively small porosity ($0.54 < \phi < 0.72$) and spherical bubbles. Unlike assumptions made by Denkov and co-workers, it was previously established experimentally that the wall slip velocity is zero for microfoams flowing in stainless steel pipes, i.e., $u_s = 0.0$ [1,22]. Finally, pipe flow viscometer is used as opposed to shear rheometer.

Table 1
Characteristics of the different Tween 20 ($\rho = 1050\,kg/m^3$ and $M = 1.227\,kg/mol$), sodium dodecyl sulfite (SDS) ($\rho = 1010\,kg/m^3$ and $M = 288.4\,g/mol$) and hexadecyltrimethy-lammonium (CTAB) ($M = 363.9\,g/mol$) solutions used in this study.

Solution	c (mM)	x (wt.%)	pH	σ (mN/m)	ϕ	r_{32} (µm)	m	$B(x)$	$C(x)$
Tween 20	0.21	0.028	4.85	41.2	0.63	47.6	0.65	0.34	0.38
Tween 20	1.71	0.22	4.53	41.5	0.68	41.9	0.62	0.40	0.44
Tween 20	4.26	0.55	4.24	39.0	0.71	36.8	0.67	0.51	0.62
Tween 20	16.77	2.17	3.94	38.8	0.72	40.8	0.66	0.70	0.86
Tween 20	32.90	4.23	3.76	38.4	0.71	39.4	0.67	0.96	1.20
Tween 20	77.77	9.96	4.28	38.9	0.70	39.0	0.6	0.95	1.24
SDS	2.803	0.081	4.86	40.9	0.65	42.8	0.66	0.66	0.67
SDS	14.03	0.398	4.50	40.82	0.69	42.0	0.66	0.72	0.76
SDS	28.06	0.780	5.34	41.45	0.70	42.2	0.62	0.62	0.78
SDS	42.09	1.194	5.36	41.32	0.65	40.8	0.63	0.65	0.79
CTAB	0.75	0.027	5.79	41.08	0.54	28.3	0.64	0.50	0.58
CTAB	1	0.037	5.64	36.47	0.59	28.0	0.66	0.61	0.65
CTAB	5	0.182	5.68	36.75	0.66	26.4	0.66	0.63	0.66

The mass fraction of the original SDS solution was 20 wt.%.

3. Experiment

The reader is referred to Ref. [1] for detailed description of the experimental setup, procedure, and data analysis. In brief, the test section consisted of a stainless steel 304 pipe with diameter D_h equal to $1.4859 \pm 0.0240\,mm$ with a 95% confidence level. The length of the pipe was 0.338 m ensuring accurate measurements of the pressure drop and fully developed laminar flow conditions [1]. The pipe diameter was previously shown to have no effect on the CGA rheology once compressibility effects have been accounted for through the volume equalization method [1,2,11,12]. Thus, only one pipe diameter was used in this study which focuses on the effect of the surfactant ionicity and concentration. Microfoam was treated as a pseudo-homogeneous time-independent non-Newtonian fluid. The pipe diameter was much larger than the bubble size so that CGA could be treated as a continuous medium [23,24]. Previous studies with stainless steel pipes of various diameter shows that the slip velocity was zero at the wall [1,22]. This was assumed to be also valid in the present study.

Microfoam was generated by stirring continuously an aqueous surfactant solution with a Silverson L4RT mixer at 7000 rpm in a baffled container [1]. The solution made from an arbitrary amount of SDS or CTAB (both from Fisher Scientific) in deionized water was continuously produced and flown through the test section. This ensured that CGA kept the same morphology and porosity as it traveled through the test section as verified experimentally [1]. The container was placed in a large tank filled with water and acting as a thermal reservoir to maintain the CGA at constant temperature. The parameters measured experimentally were (i) the pressure drop along the channel ΔP, (ii) the microfoam temperature, (iii) the volumetric flow rate $\dot{Q}$, (iv) the mass flow rate $\dot{m}$, (v) the porosity ϕ, (vi) the bubble size distribution and the Sauter mean bubble radius r_{32}, as well as (vii) the surface tension σ of the surfactant solution/air interface, and (viii) the solution pH.

The wall shear stress τ_w and the apparent shear rate $\dot{\gamma}_a$ were determined experimentally according to [2,11],

$$\tau_w = \frac{D_h \Delta P}{4L} \quad \text{and} \quad \dot{\gamma}_a = \frac{32\dot{Q}}{\pi D_h^3} \tag{9}$$

where D_h is the hydraulic diameter, ΔP is the pressure drop measured between the inlet and outlet of the pipe separated by a distance L, and $\dot{Q}$ is the volumetric flow rate.

Error analysis was performed as reported in Ref. [1]. The uncertainty in porosity $\Delta\phi/\phi$ was estimated at about 7%. For CGA made of SDS and CTAB subjected to apparent shear rate $\dot{\gamma}_a$ less than $2000\,s^{-1}$, the measured pressure drop oscillated significantly and experimental uncertainties associated with τ_w and $\dot{\gamma}_a$ were large.

Thus, we considered only data for shear rate larger than $2000\,s^{-1}$ with experimental uncertainty $\Delta\tau_w/\tau_w$ and $\Delta\dot{\gamma}_a/\dot{\gamma}_a$ less than 15 and 7%, respectively.

Finally, the setup, sensors calibration, and analysis (see Ref. [1]) were successfully validated by measuring the viscosity of deionized water and comparing it with values obtained from the thermophysical properties database DIPPR [25]. It establishes that the measured viscosity of deionized water fell within 7.4% of that reported in the literature and equal to 0.927 mPa s at 23 °C [25].

4. Results and discussion

4.1. Solution characteristics and CGA morphology

Table 1 summarizes the characteristics of the Tween 20 [1], SDS, and CTAB solutions and the corresponding microfoams investigated in this study. It includes the surfactant mass fraction x (in wt.%) and molar concentration c (in mM/L), the surface tension σ, the pH, the Sauter mean bubble radius r_{32}, and the average porosity ϕ. All variables were measured before each experimental run and averaged. The porosity ranged from 0.54 to 0.70 for SDS and CTAB solutions. In all cases, it was verified that no appreciable changes could be observed in both the porosity and the bubble size distribution between the inlet and outlet of the test section. The CGA temperature was 25 ± 2 °C. The absolute operating pressure was about 1 atm for all runs.

Fig. 1 shows τ_w versus $\dot{\gamma}_a$ for the different single phase surfactant solutions used in this study. It indicates that all surfactant solutions had approximately the same viscosity as deionized water. In addition, Fig. 2 illustrates representative photographs of microfoams made from SDS and CTAB solutions with the lowest and largest concentrations considered. It shows closely packed spherical bubbles and justifies why the term "microfoams" is used despite the fact that the porosity varies between 0.54 and 0.72. Fig. 3 shows the associated bubble size distribution measured from 130 to 240 individual bubbles using the image analysis software Image J. Micrographs of CGA were taken under a Leica DM IL microscope within 1 min of being sampled from the baffled container. From both Figs. 2 and 3, it is evident that the bubble size distribution narrows as the surfactant concentration increases. This was also observed with Tween 20 [1]. The Sauter mean bubble radius r_{32} obtained with SDS decreases from 42.8 to 40.8 µm as the concentration increased from 0.081 to 1.194 wt.%. Simultaneously, the porosity increased from 0.65 to 0.70 and the microfoam was more and more stable. This can be attributed to the decrease in surface tension and to the increased availability of surfactant molecules to adsorb at the bubble surface and stabilize it. Similar trend was observed with CTAB. However,
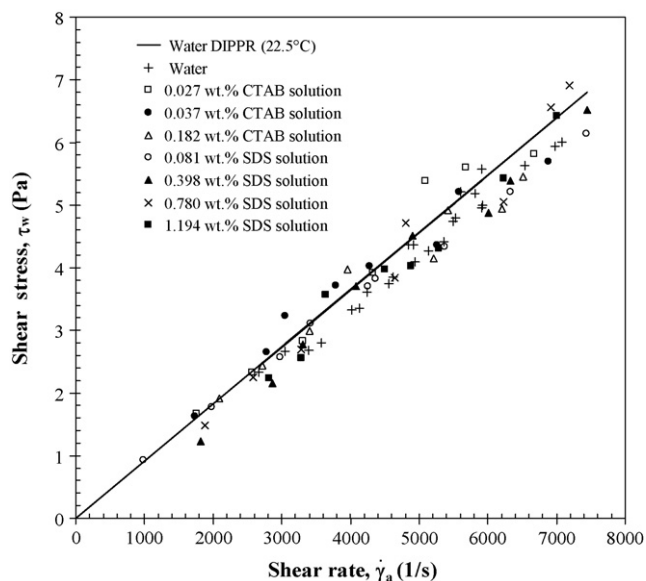
Fig. 1. Shear stress versus shear rate measured for deionized water and aqueous solutions of SDS and CTAB at various concentrations.

the Sauter mean bubble radius for CTAB microfoams was smaller than that of SDS or Tween 20 and varied between 28.3 and 26.4 μm.

4.2. Rheology

The effect of SDS and CTAB concentration on CGA rheology was assessed with aqueous solutions of SDS at mass fractions 0.081, 0.398, 0.780, 1.194 wt.% and of CTAB at mass fractions 0.027, 0.037, and 0.182 wt.%. Figs. 4 and 5 show the volume equalized shear stress τ_w/ε as a function of the volume equalized apparent shear rate $\dot{\gamma}_a/\varepsilon$ for the above SDS and CTAB solutions, respectively. As observed with Tween 20 [1], experimental data points become less scattered and more consistent as the surfactant concentration increases

thanks to more stable CGA. Both Figs. 4 and 5 indicate that the CGA can be considered as a shear thinning fluid in terms of volume equalized apparent shear rate and shear stress with empirical constants depending on the type of surfactant and its concentration. Figs. 4 and 5 also establish that, for a given value of $\dot{\gamma}_a/\varepsilon$, the volume equalized shear stress τ_w/ε increases with surfactant concentration up to a maximum value beyond which it is independent of concentration. This was also reported in the literature [1,26]. This cannot be attributed to changes in the solution viscosity (Fig. 1) or in surface tension since neither varies significantly over the range of surfactant mass fractions considered (Table 1). The increase in τ_w/ε with surfactant concentration is likely due to the reduction in the maximum packing of spherical bubbles as their size distribution narrows [1,27] and possibly to the hypothetical shell structure of CGA bubbles becoming thicker with increasing surfactant concentration [28].

4.3. Dimensional analysis

In order to generalize the results, the volume equalized apparent shear rate and shear stress are made dimensionless through the use of volume equalized Capillary number Ca^* and dimensionless shear stress τ_w^* expressed respectively as,

$$Ca^* = \frac{\mu_\ell r_{32} \dot{\gamma}_a}{\varepsilon \sigma} = Ca/\varepsilon \quad \text{and} \quad \tau_w^* = \frac{\tau_w r_{32}}{\sigma \varepsilon} \tag{10}$$

First, a power–law relationship was assumed between Ca^* and τ_w^* for its capability to fit a wide range of data and as suggested by theoretical models [16,19], i.e.,

$$\tau_w^* = B(x)(Ca^*)^m \tag{11}$$

Fig. 6 shows the evolution of the power–law index m as a function of surfactant mass fraction x for SDS, CTAB, and Tween 20 [1]. It establishes that m was nearly constant for all concentrations and surfactants considered. The average value of the power–law index m was found to be 0.64 ± 0.04 with 95% confidence interval. Note also that the surface dilational modulus of aqueous SDS [16] and CTAB
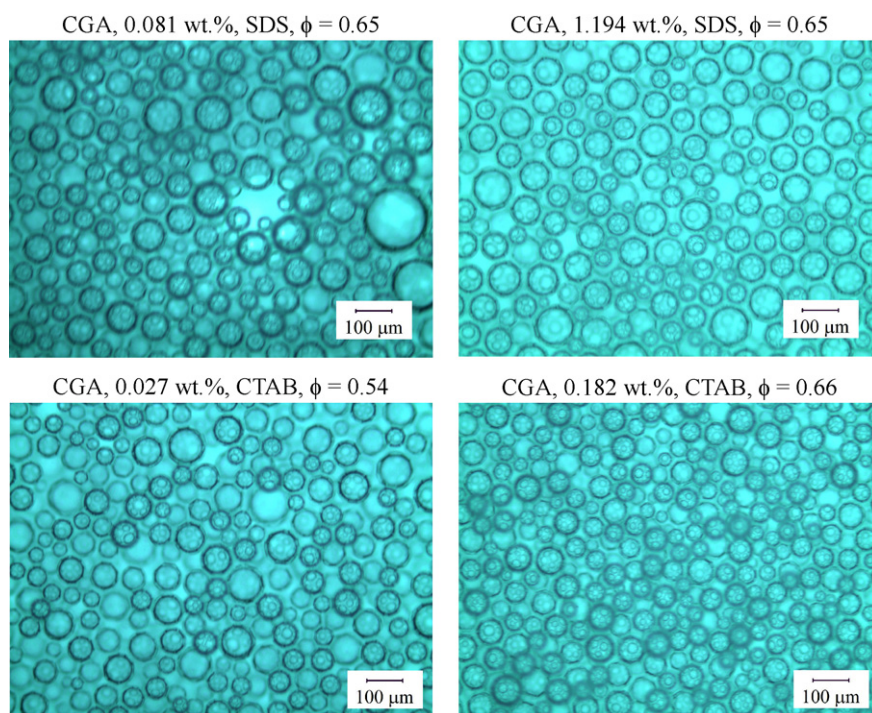
Fig. 2. Typical micrograph of CGA formed with different aqueous solutions of SDS (top) and CTAB (bottom) at $25 \pm 2\,^\circ$C.
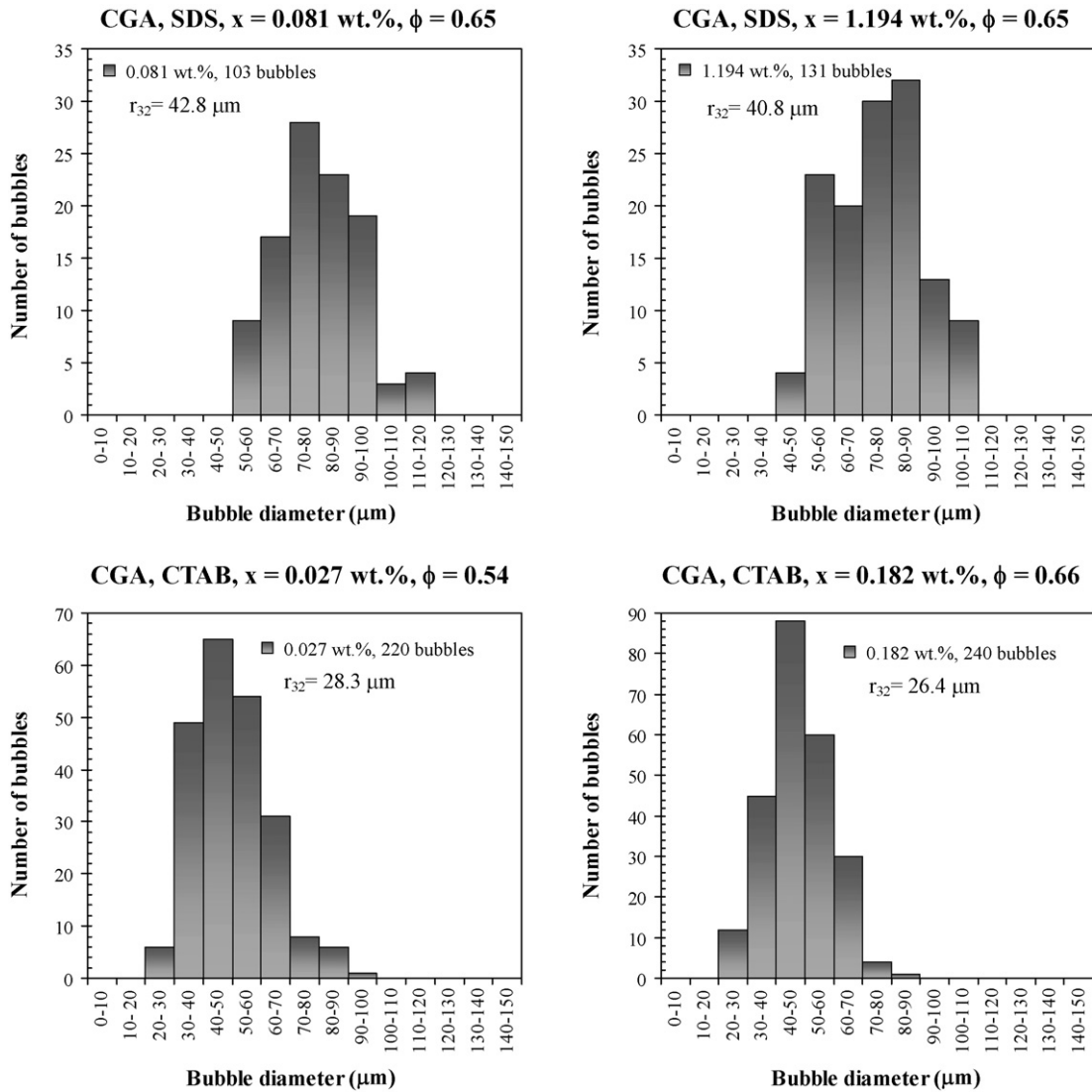
Fig. 3. Bubble size distribution of CGA formed with different SDS and CTAB aqueous solutions at $25 \pm 2\,^{\circ}C$ corresponding to micrographs shown in Fig. 2.
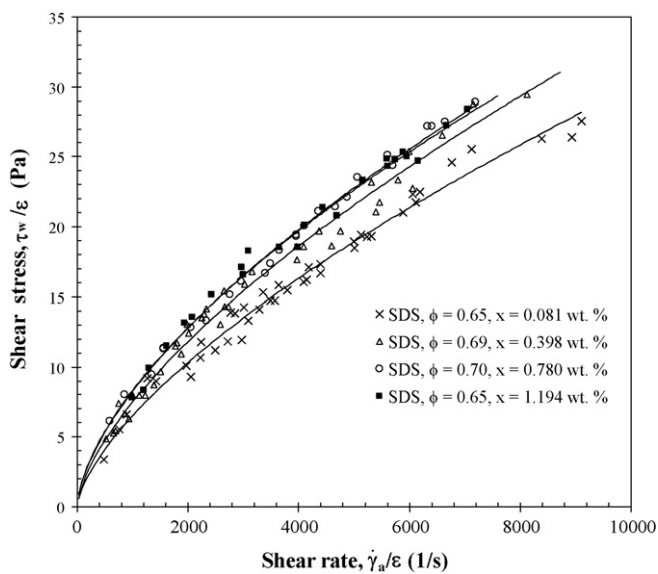
Fig. 4. Volume equalized shear stress versus shear rate for CGA made from SDS aqueous solution with different concentrations obtained in the 1.5 mm diameter pipe at $25 \pm 2\,^{\circ}C$.

Fig. 5. Volume equalized shear stress versus shear rate for CGA made from CTAB aqueous solution with different concentrations obtained in the 1.5 mm diameter pipe at $25 \pm 2\,^{\circ}C$.

Author's personal copy

98 *J. Zhao et al. / Colloids and Surfaces A: Physicochem. Eng. Aspects 348 (2009) 93–99*
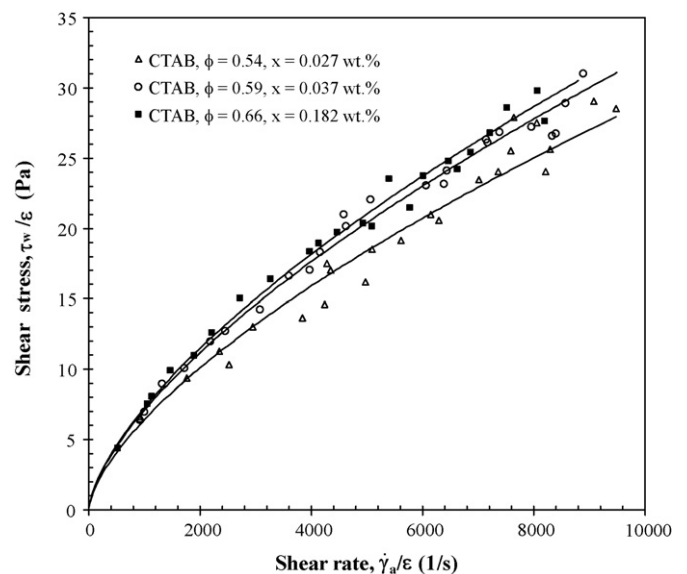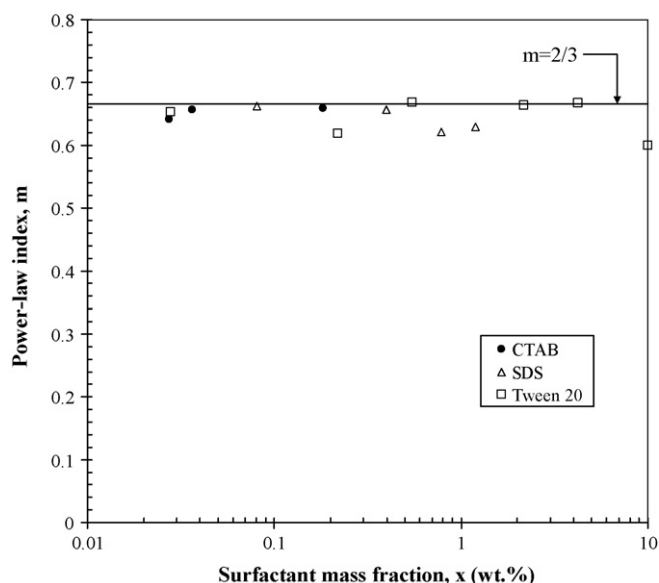
Fig. 6. Empirical power–law index m as a function of surfactant mass fraction x obtained in the 1.5 mm diameter pipe at 25 ± 2 °C for microfoams made of SDS, CTAB, and Tween 20. Solid line corresponds to $m = 2/3$.

[29–31] in air is small and less than 60 mN/m suggesting that the bubble surfaces are tangentially mobile. Thus, experimental results for microfoams with spherical bubbles and porosity ranging from 0.54 to 0.72 are consistent with the theoretical models assuming large porosity, non-spherical bubbles, and non-zero slip velocity [16,19] as well as experimental data for a train of large polyhedral bubbles [17].

Similarly, the empirical coefficient $B(x)$ did not vary significantly with concentration and was almost identical for SDS and CTAB (see Table 1). The average value of $B(x)$ for large surfactant concentrations of SDS and CTAB was equal to 0.65 ± 0.09. For Tween 20, $B(x)$ was found to increase with concentration. Note that $B(x)$ for Tween 20 was erroneously reported in our previous study (Ref. [1], Fig. 10).

Finally, Figs. 7 and 8 show τ_w^* versus $(Ca^*)^{2/3}$ for microfoams made from SDS and CTAB solutions with various concentrations.
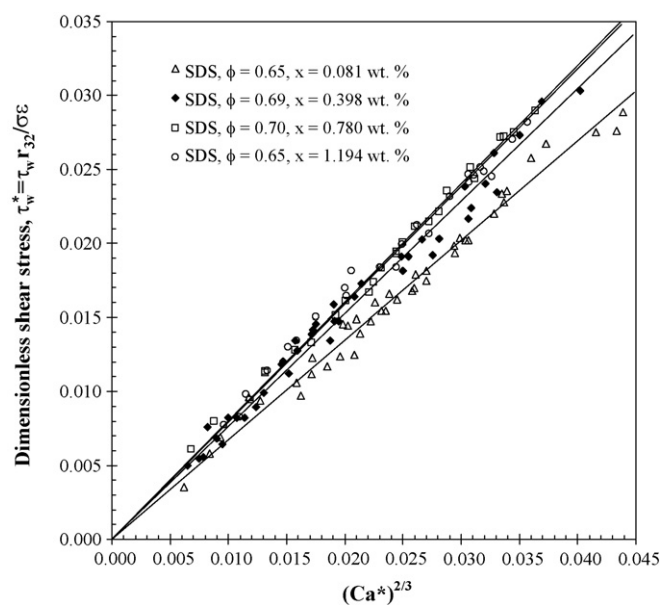
Fig. 7. Dimensionless volume equalized wall shear stress τ_w^* versus $(Ca^*)^{2/3}$ for CGA made from SDS aqueous solution with different concentrations.
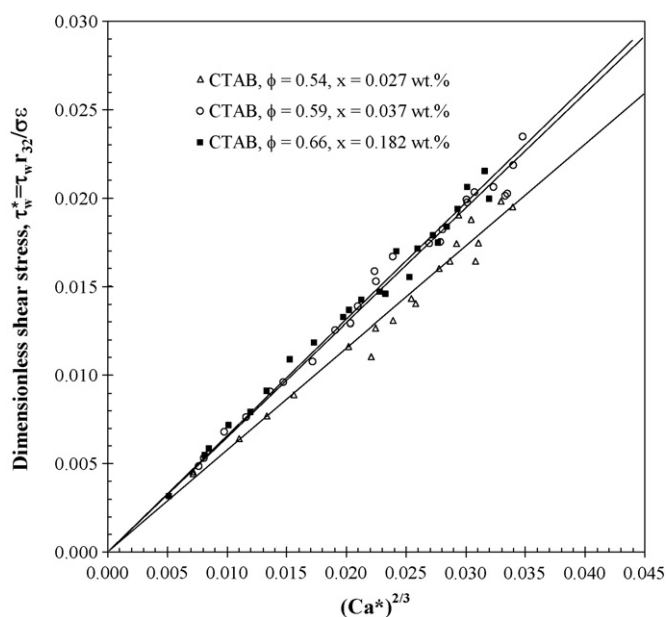
Fig. 8. Dimensionless volume equalized wall shear stress τ_w^* versus $(Ca^*)^{2/3}$ for CGA made from CTAB aqueous solution with different concentrations.

Both show a linear relationship between τ_w^* and $(Ca^*)^{2/3}$ as observed with Tween 20 [1]. In other words, $\tau_w^* = C(x)(Ca^*)^{2/3}$ where the coefficient of proportionality $C(x)$ increases with concentration until it reaches a maximum value. This also agrees well with results obtained with Tween 20 [1]. The values of the parameter $C(x)$ are summarized in Table 1. It is of the order of unity and increases with surfactant mass fraction x. However, quantitative relationship between $C(x)$ accounting for the effect of concentration and the type of surfactants is not obvious and will not be sought. The same conclusions can be reached when $C(\phi)$ is plotted as function of porosity (not shown).

5. Conclusion

This study focused on the rheology of microfoams made with aqueous solutions of Tween 20, SDS, and CTAB at various concentrations featuring (i) closely packed spherical bubbles, (ii) porosity ranging from 0.54 to 0.72, and (iii) Sauter mean radius between 26.4 and 47.6 μm. The following conclusions can be drawn:

1. CGA can be treated as a shear thinning fluid for all the surfactant solutions considered.
2. The dimensionless volume equalized shear stress τ_w^* is proportional to the volume equalized Capillary number Ca^* raised to a power–law index m between 0.6 and 0.66 which is closed to 2/3.
3. The results are consistent with different theoretical and experimental studies for foams with larger porosity, non-spherical bubbles, and/or non-zero wall slip velocity [16,17,19].
4. Increasing the surfactant concentration causes the shear stress to increase for a given apparent shear rate. This is likely due to the associated reduction in polydispersity of the bubbles.

Acknowledgments

J. Zhao et al. / Colloids and Surfaces A: Physicochem. Eng. Aspects 348 (2009) 93–99

99

References

[1] S. Larmignat, D. Vanderpool, H. Lai, L. Pilon, Rheology of colloidal gas aphrons (microfoams), Colloids and Surfaces A: Physicochemical and Engineering Aspects 322 (1–3) (2008) 199–210.

[2] P. Valko, M.J. Economides, Volume equalized constitutive equations for foamed polymer solutions, Journal of Rheology 36 (1992) 111–127.

[3] D. Roy, K.T. Valsaraj, W.D. Constant, M. Darji, Removal of hazardous oily waste from a soil matrix using surfactants and colloidal gas aphron suspensions under different flow conditions, Journal of Hazardous Materials 38 (1994) 127–144.

[4] D. Roy, R.R. Kommalapati, K.T. Valsaraj, W.D. Constant, Soil flushing of residual transmission fluid: application of colloidal gas aphron suspensions and conventional surfactant solutions, Water Research 29 (1995) 589–595.

[5] M. Ali Hashim, B. Sen Gupta, The application of colloidal gas aphrons in the recovery of fine cellulose fibres from paper mill wastewater, Bioresource Technology 64 (3) (1998) 199–204.

[6] E. Fuda, P. Jauregi, An insight into the mechanism of protein separation by colloidal gas aphrons (CGA) generated from ionic surfactants, Journal of Chromatography B 843 (2) (2006) 317–326.

[7] P. Jauregi, J. Varley, Colloidal gas aphrons: potential applications in biotechnology, Trends in Biotechnology 17 (10) (1999) 389–395.

[8] F.A. Morrison, Understanding Rheology, Oxford University Press, Oxford, UK, 2001.

[9] R. Höhler, S. Cohen-Addad, Rheology of liquid foams, Journal of Physics: Condensed Matter 17 (2005) R1041–R1069.

[10] B. Herzhaft, S. Kakadjian, M. Moan, Measurement and modeling of the flow behavior of aqueous foams using a recirculating pipe rheometer, Colloids and Surfaces A: Physicochemical and Engineering Aspects 263 (2005) 153–164.

[11] C. Enzendorfer, R.A. Harris, P. Valko, M.J. Economides, P.A. Fokker, D.D. Davies, Pipe viscometry of foams, Journal of Rheology 39 (2) (1995) 345–356.

[12] W. Winkler, P. Valko, M.J. Econmides, Laminar and drag-reduced polymeric foam flow, Journal of Rheology 38 (1) (1994) 111–127.

[13] L.W. Schwartz, H.M. Princen, A theory of extensional viscosity for flowing foams and concentrated emulsion, Journal of Colloidal and Interface Science 118 (1) (1987) 201–211.

[14] F.P. Bretherton, The motion of long bubbles in tubes, Journal of Fluid Mechanics 10 (1961) 166–188.

[15] H.M. Princen, A.D. Kiss, Rheology of foams and highly concentrated emulsions. IV. An experimental study of shear viscosity and yield stress of concentrated emulsions, Journal of Colloidal and Interface Science 128 (1989) 176–187.

[16] N.D. Denkov, V. Subramanian, D. Gurovich, A. Lips, Wall slip and viscous dissipation in sheared foams: effect of surface mobility, Colloids and Surfaces A: Physicochemical and Engineering Aspects 263 (2005) 129–145.

[17] I. Cantat, N. Kern, R. Delannay, Dissipation in foam flowing through narrow channels, Europhysics Letters 65 (5) (2004) 726–732.

[18] E. Terriac, J. Etrillard, I. Cantat, Viscous force exerted on a foam at a solid boundary: influence of the liquid fraction and of the bubble size, Europhysics Letters 74 (5) (2006) 909–915.

[19] N.D. Denkov, S. Tcholakova, K. Golemanov, V. Subramanian, A. Lips, Foam–wall friction: effect of air volume fraction for tangentially immobile bubble surface, Colloids and Surfaces A: Physicochemical and Engineering Aspects (282–283) (2006) 329–347.

[20] K. Golemanov, N.D. Denkov, S. Tcholakova, M. Vethamuthu, A. Lips, Surfactant mixtures for control of bubble surface mobility in foam studies, Langmuir 24 (18) (2008) 9956–9961.

[21] H. Tseng, L. Pilon, Rheology and convective heat transfer properties of colloidal gas aphrons in horizontal minichannels, International Journal of Heat and Fluid Flow 27 (2) (2006) 298–310.

[22] P.C. Harris, V.G. Reidenbach, High-temperature rheological study of foam facturing fluids, Journal of Petroleum Technology 39 (5) (1987) 613–619.

[23] J.P. Heller, M.S. Kuntamukkula, Critical review of the foam rheology literature, Industrial & Engineering Chemistry Research 26 (2) (1987) 318–325.

[24] R.K. Prud'homme, S.A. Khan, Experimental results on foam rheology in foams: theory, measurements, and applications, in: R.K. Prud'homme, S.A. Khan (Eds.), Surfactant Science Series, vol. 57, Marcel Dekker, New York, NY, 1996, pp. 217–242.

[25] Thermophysical Properties Database DIPPR 801, http://dippr.byu.edu/database.asp.

[26] R.C.G. Oliveira, J.F. Oliveira, B.M. Moudgil, Optimizing micro-foam rheology for soil remediation, Progress in Colloid Polymer Science 128 (2004) 298–302.

[27] J.J. Stickel, R.L. Powell, Fluid mechanics and rheology of dense suspensions, Annual Review of Fluid Mechanics 37 (2005) 129–149.

[28] F. Sebba, Foams and Biliquid Foams-Aphrons, John Wiley & Sons, New York, 1987.

[29] K.D. Wantke, H. Fruhner, J. Ortegren, Surface dilatational properties of mixed sodium dodecyl sulfate/dodecanol solutions, Colloids and Surfaces A: Physicochemical and Engineering Aspects 221 (2003) 185–195.

[30] F. Monroy, J. Giermanskahan, D. Langevin, Dilational viscoelasticity of surfactant monolayers, Colloids and Surfaces A: Physicochemical and Engineering Aspects 143 (1998) 251–260.

[31] H. Fruhner, K.-D. Wantke, K. Lunkenheimer, Relationship between surface dilational properties and foam stability, Colloids and Surfaces A: Physicochemical and Engineering Aspects 162 (1999) 193–202.